15th AIAA/CEAS Aeroacoustics Conference (30th AIAA Aeroacoustics Conference)
11 - 13 May 2009, Miami, Florida

AIAA 2009-3316

Matched hybrid approaches to predict jet noise by using Large-Eddy Simulation

Guillaume Bodard*

SNECMA, Acoustics Department, 77550 Moissy-Cramayel, France

Christophe Bailly†

LMFA, Ecole Centrale de Lyon, 69134 Ecully, France

François Vuillot‡

ONERA, 92322 Chatillon, France

An hybrid acoustic method combining a large eddy simulation and a stastistical modelling of turbulent noise sources is developed to predict noise of real jets. The main objective is to merge advantages of both kind of prediction model to obtain a robust industrial acoustic tool. Thus, the Ffowcs-Williams & Hawkings Wave Extrapolation Method is classically used to obtain the low frequency part of spectra. The higher frequency part is estimated by means of Tam & Auriault's fine-scale turbulence noise theory applied to a reconstructed unfiltered mean flow field. This hybrid jet noise prediction method as well as aeroacoustics results for isothermal and heated subsonic jets ($M = 0.9$) are reported in this paper. An overestimation of turbulence levels in mixing layers is observed, leading to a shorter potential core for both simulations. However, velocity profiles and turbulence length scales are satisfactory by using normalized distances by the potential core length. Noise levels obtained are consequently overpredicted even if angular variations and temperature effects seem well evaluated.

I. Introduction

Aircraft jet noise has been notably reduced since the beginning of commercial jets, but it still remains the dominant source at take-off[13]. An accurate jet noise prediction tool is thus essential to engine manufacturers for certification purposes. Since Lighthill's theory[20] in the fifties, the Reynolds-Averaged Navier-Stokes (RANS) equations are now commonly solved in industry, and are used as input data to predict jet noise for conventional nozzle geometries, see Bailly *et al.*[2], Tam & Auriault[29], Morris & Farassat[23] or Khavaran & Bridges[17] among others. However, complex nozzle designs such as lobed mixer systems or chevron cannot been discriminated by these approaches. Only time-dependant simulations seem able to correctly reproduce changes in the turbulent field and consequently in the radiated sound field.

In the present work, large-eddy simulations (LES) are performed to describe a part of the turbulent flow, namely low-frequency spatial scales in the free shear flow and also high-frequency scales directly linked to mixing devices at the nozzle exit. Noise of these contributions is directly obtained through the use of a wave extrapolation method. Fine-scale turbulence is of course missing, and a statistical modelling is thus derived to take account of this high-frequency component in acoustic spectra. The methodology proposed in this paper aims to evaluate both contributions for subsonic jet noise. LES data are used as input in Tam & Auriault's model[29] and also in Ffowcs-Williams & Hawkings method[10].

The paper is organized as follows. The coupling procedure is discussed in section II and computational parameters are provided in section III. Then, aerodynamic and acoustic results are discussed in section IV and V respectively. Concluding remarks are finally given in section VI.

*PhD Student, *guillaume.bodard@snecma.fr*
†Professor, Senior Member AIAA, *christophe.bailly@ec-lyon.fr*
‡Assistant director, CFD and aeroacoustics department, Senior Member AIAA, *Francois.Vuillot@onera.fr*

II. Strategy for acoustic predictions

The acoustic prediction method developed in the present work combines two existing methodologies: the Wave Extrapolation Method (WEM) of Ffowcs-Williams & Hawkings[10] (FWH) and the fine-scale turbulence noise model proposed by Tam & Auriault[29].

Applied to unsteady computations such as LES, the first one is appropriate to evaluate far field noise by means of near field fluctuating data stored over a control surface enclosing all acoustic sources. Thus, this method provides the noise contribution of large turbulent structures resolved by the computation, namely noise for frequencies lower than the cut-off frequency linked to mesh refinement and numerical scheme accuracy. In addition to the large scale noise, the low frequency component of fine scale noise is also included. Tam & Auriault's prediction method is then used to estimate the high-frequency part of the turbulent field, with respect to the local mesh. Mean fields calculated from LES are employed, and the unresolved part of the kinetic energy is modeled. Moreover, the low frequency part of far field spectra, already directly evaluated by the WEM, is removed with a local frequency filtering. Note also that the interaction between the two fields is not considered in what follows.

The power spectral density S can then be decomposed as $S(\mathbf{x},\omega) = S_{\mathrm{LF}}(\mathbf{x},\omega) + S_{\mathrm{HF}}(\mathbf{x},\omega)$, with S_{LF} and S_{HF} respectively the low and high frequency contributions.

II.A. Wave extrapolation method for low frequency component

The Wave Extrapolation Method of Ffowcs-Williams & Hawkings[10] is used to obtain far field pressure signals. The resolved quantities $\overline{p}$, $\overline{\rho}$ and $\widetilde{u}_i$ are then stored over a acoustic control surface enclosing jet noise sources. In the present case, the surface is static and assuming that source terms are negligible outside the control surface, the acoustic pressure p'_{FWH} can be expressed as:

$$4\pi p'_{\mathrm{FWH}}(\mathbf{x},t) \approx \frac{\partial}{\partial t}\iint_{\Sigma}\left[\frac{\overline{\rho}\widetilde{u}_n}{r}\right]_{\tau^*} d\Sigma \quad + \quad \frac{1}{c_0}\frac{\partial}{\partial t}\iint_{\Sigma}\left[\frac{r_i\widetilde{P}_{ij}n_j + \overline{\rho}\widetilde{u}_i r_i \widetilde{u}_n}{r^2}\right]_{\tau^*} d\Sigma \tag{1}$$

where $\widetilde{P}_{ij} = (\overline{p}-p_0)\delta_{ij} - \widetilde{\tau}_{ij}$, $r = |\mathbf{r}|$ is the source-observer distance and n_i is the surface normal vector.

This method has been implemented with the advanced-time approach, refer to Brentner *et al.*[7] for rotor noise evaluation or more recently to Casalino[8]. The low frequency component of the power spectral density S_{LF} is then obtained, the cut-off frequency being determined by mesh refinement and numerical scheme accuracy.

II.B. Fine-scale turbulence noise model for high frequency component

II.B.1. Tam & Auriault's model

Tam & Auriault[29] have developed a new acoustic analogy to predict fine-scale contribution of jet noise. This method requires as input data the mean flow field and two turbulence scales. The acoustic power spectral density of fine-scale turbulence $S_{\mathrm{T\&A}}$ for a far field observer position $\mathbf{x}$ is given by:

$$S_{\mathrm{T\&A}}(\mathbf{x},\omega) = 4\pi\left(\frac{\pi}{\log 2}\right)^{3/2}\iiint \frac{\hat{q}_s^2 l_s^3}{c^2\tau_s}\left|p_a(\mathbf{x}_2,\mathbf{x},\omega)\right|^2 \frac{\exp\left\{-\omega^2 l_s^2/4u_c^2\log 2\right\}}{\left[1+\omega^2\tau_s^2\left(1-u_c\cos\theta/a_\infty\right)^2\right]}d\mathbf{x}_2 \tag{2}$$

with $\mathbf{x}_2$ the source position in the jet volume, p_a the adjoint pressure, u_c the convection velocity, $\tau_s = c_\tau k_t/\epsilon$ and $l_s = c_l k_t^{3/2}/\epsilon$ the time and space turbulent scales and $\hat{q}_s^2/c^2 = A^2\left(2/3\overline{\rho}k_t\right)^2$ the elementary source intensity. Here, k_t stands for the turbulent kinetic energy and ϵ for its turbulent dissipation rate.

The determination of p_a is generally obtained by solving the adjoint problem. But, as noted by Tam[31] and Morris & Farassat,[23] the adjoint pressure in the transverse direction takes a simple analytical form:

$$\left|p_a(\mathbf{x}_2,\mathbf{x},\omega)\right|^2 = \frac{\omega^2}{64\pi^4 c_0^4\left|\mathbf{x}-\mathbf{x}_2\right|^2} \tag{3}$$

To simplify our methodology, the exact solution is computed for $\theta = 90°$ radiation and the angular evolution is then taken into account thanks to a directivity factor $(1 - M_c \cos\theta)^{-3}$ proposed initially by Goldstein[12] and used by Morris & Farassat[23]. This simplication is however not valid in the cone of silence, where refraction effects become dominant.

II.B.2. Adaptation to LES mean flow field

In order to apply the fine-scale turbulence noise model, the turbulent kinetic energy and its dissipation rate have to be evaluated. In particular, the unsolved part of kinetic energy k_{sgs} must be estimated. A formulation similar to Smagorinsky's subgrid scale model[27] is applied. The turbulent kinetic energy k_t writes as $k_t = k_{\text{LES}} + k_{\text{sgs}}$, where:

$$k_{\text{LES}} = \frac{\langle \widetilde{u}_i'' \widetilde{u}_i'' \rangle}{2} = \frac{\langle \widetilde{u}_i \widetilde{u}_i \rangle - \langle \widetilde{u}_i \rangle^2}{2} \tag{4}$$

$$k_{\text{sgs}} = 2 C_I \Delta^2 \langle \widetilde{s}_{ij} \rangle \langle \widetilde{s}_{ij} \rangle \quad \text{where} \quad \langle \widetilde{s}_{ij} \rangle = \frac{1}{2} \left(\frac{\partial \langle \widetilde{u}_i \rangle}{\partial x_j} + \frac{\partial \langle \widetilde{u}_j \rangle}{\partial x_i} \right) \tag{5}$$

and with $\widetilde{u}_i''$ the fluctuating part of the resolved velocity $\widetilde{u}_i$, that is $u_i = \widetilde{u}_i + \widetilde{u}_i''$. C_I is Smagorinsky's constant and Δ is the local mean grid size. Moreover, the turbulent dissipation rate ϵ, linked to unsolved turbulent structures, is determined using the turbulent kinetic energy and the radial gradient of the mean axial velocity, which yields:

$$\epsilon = c_\epsilon k_t \frac{d \langle \widetilde{u}_1 \rangle}{dr} \tag{6}$$

Turbulent scales and source intensities can thus be calculated to evaluate the acoustic power spectral density associated with fine-scale noise.

II.B.3. Frequency filtering

Tam & Auriault's theory provides acoustic levels from mixing noise due to fine scale turbulence. However, the low frequency part of this contribution is already evaluated thanks to the FWH method. Thus, this low frequency fine scale turbulence noise has to be removed. A local frequency filtering procedure has been developed and is now described.

The main objective is to identify if the mesh between the source location and the acoustic surface is refined enough to propagate the considered acoustic wave without significant numerical dissipation. Thus, in each grid cell, a mean grid size $\Delta_j(\mathbf{x})$ until the acoustic surface S_j is estimated, using the number of radial grid cells $N_j(\mathbf{x})$ and their respective characteristic size $\Delta(\mathbf{x}_i)$. The mean grid size is then determined as follows:

$$\Delta_j(\mathbf{x}) = \frac{1}{N_j(\mathbf{x})} \sum_{i=1}^{N_j(\mathbf{x})} \Delta(\mathbf{x}_i) \quad \text{with} \quad \Delta(\mathbf{x}_i) = \sqrt[3]{Vol(\mathbf{x}_i)} \tag{7}$$

where $Vol(\mathbf{x}_i)$ is the volume of the ith cell.

A preliminary study on plane wave propagation was performed to investigate the dissipation induced by numerical schemes. The main issue of this work is that 30 points per wavelength are necessary to solve accurately wave propagation. A critical wavelength can then be determined as $\lambda_c(\mathbf{x}_i) = 30\Delta_j(\mathbf{x}_i)$. And the contribution estimated by the fine-scale turbulence noise model can be included if the mesh is not enough refined to directly evaluate this part using the FWH method.

III. Computational parameters

III.A. Jets parameters

The single stream free jets computed in this paper were investigated in JEAN (*Jet Exhaust Aerodynamics & Noise*) european program. This simple geometry is a first step to evaluate our prediction methodology before performing computations of more realistic exhausts. Large Eddy Simulations have already been performed on this geometry by Andersson *et al.*[1], Bogey *et al.*[6] or more recently by McMullan *et al.*[22] and Huet *et al.*[14] Two subsonic jets are considered in this study. The exhaust diameter is $D = 0.05\,\mathrm{m}$ and the Mach number $\mathrm{M} = 0.9$ is quite comparable to commercial engine exhaust flows. Simulation parameters are detailed in Table 1.

	M	$\mathrm{T_j/T_0}$	$\mathrm{Re_D}$	$\mathrm{Q_m}$ [kg/s]
jet1 - isothermal	0.9	1	1.1×10^6	0.725
jet2 - heated	0.9	2	3.2×10^5	0.403

Table 1. Exhaust conditions of jet1 and jet2.

III.B. Mesh

The goal of this study is to develop an industrial noise prediction methodology able to deal with complex geometries. Consequently, the mesh size must be reasonable in order to keep similar design criteria for further computations of more realistic exhausts such as dual-stream nozzles.

Two very different mesh criteria have to be considered. Firstly, a maximum cell size has to be determined to ensure accurate wave propagation. It is directly linked to numerical schemes properties and frequency resolution needed. Preliminary test cases were performed with an explicit Runge-Kutta second order time scheme combined with a third order upwind spatial scheme to evaluate the number of points per wavelength necessary to solve acoustic propagation without significant dissipation. About 30 points per wavelength are found sufficient. Moreover, the peak frequency of jet noise is observed for Strouhal numbers between 0.2 and 0.3, as mentioned by Tam *et al.*[32] Thus, our mesh is designed to solve accurately acoustic waves up to St= 0.5.

An other crucial choice concerns the mesh refinement on wall boundaries, to correctly evaluate the mixing in the shear layers. As pointed out by Zaman, the momentum thickness order of magnitude for high Reynolds numbers ($Re \approx 10^6$) is $\delta_\theta/D \approx 0.001$. However, roughly 20 points are necessary to correctly discretize this length scale and such a value then leads to huge meshes, even for simple geometries. Thus, a higher ratio of 0.01 - 0.05 is usually chosen for LES, as for Bogey *et al.*[4,5], Lew *et al.*[18], Bodony *et al.*[3] or Zhao *et al.*[35] In our case, the mesh size on walls is designed to discretize with 20 points a momentum thickness value of $\delta_\theta/D = 0.05$, yielding to $\Delta r/D = 0.002$.

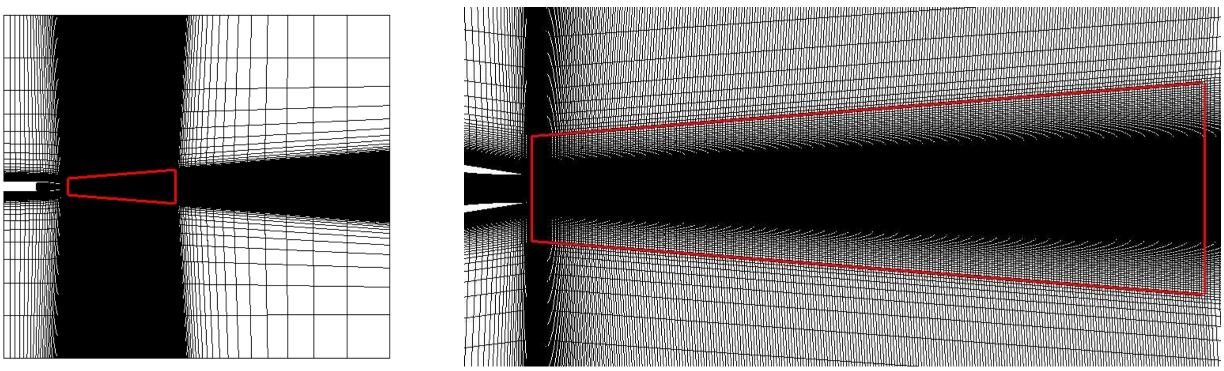

Figure 1. Mesh cut plane. —— **boundaries of the refined zone.**

To ensure an accurate sound propagation, the refined zone extends $25\,D$ downstream and from $2\,D$ to $4.5\,D$ radially (see Figure 1). Mesh cells are then stretched to $75\,D$ downstream, $15\,D$ upstream and $40\,D$ radially, to avoid wave reflections on boundaries. 60 cells are finally displayed in the azimuthal direction. The final mesh used for both LES then counts 3 million cells.

III.C. Numerical procedure

Large Eddy Simulations are performed with the unstructured parallel Navier-Stokes solver CEDRE developed by ONERA[21]. Both jets are computed without subgrid-scale model, as proposed for instance by Shur *et al.*[28] Indeed, for "coarse" LES, numerical dissipation order of magnitude is higher than modelized dissipation and subgrid-scale model is useless.

The numerical procedure can be decomposed in 3 steps. Firstly, 50 iterations are performed with a first-order implicit time scheme to initialize the flow in the exhaust. Then, the time step for all the simulation is chosen in order to ensure CFL<1 in all the computational domain. In our case, such a criterion leads to $\Delta t = 0.35\,\mu$s, so $\Delta t^* = \Delta t\, U_j/D = 2.13\times 10^{-3}$. Explicit Runge-Kutta second order time scheme is combined with a third order upwind spatial scheme to continue the simulations. To install the flow in the domain, 100 000 iterations are carried out, corresponding to a total time $T = 210\,D/U_j$. Finally, 175 000 iterations are performed, with a storage of jet flow properties on control surfaces for acoustic post-processing. Mean flow properties are also computed during these last iterations. This corresponds to a period $T = 360\,D/U_j$. To avoid huge data storage, surface quantities are written every 20 time steps, the sampling frequency still being high enough to satisfy Nyquist criterion for considered frequencies. Each simulation has been performed in 72 hours on 64 Itanium processors (Platine-CCRT).

IV. Aerodynamic results

IV.A. Mean flow field

First investigations are made on potential core length x_c, estimated as the axis length on which the axial mean velocity $\langle \widetilde{u}_1 \rangle$ verifies $\langle \widetilde{u}_1 \rangle / U_j > 0.95$. As summed up in Table 2, a non negligible underestimation of this length of 30% is observed for jet1 and jet2 in comparison to Jordan *et al.*[15] experiments. Such a phenomenon was expected, because momentum thickness is quite larger in the simulation than in experiments. Thus, turbulent eddies sizes are overestimated and so are the turbulent levels. Then, mixing process in the shear layer is faster and leads to shorten the potential core. Similar tendancies have been observed in other LES, refer to Andersson *et al.*[1], Bogey *et al.*[6] or Huet *et al.*[14] In the present simulations, mesh refinement is especially too poor in the azimuthal direction with respect to other components. Indeed, at the nozzle lip, the azimuthal size is 25^{th} as big as the radial size and 5^{th} as big as the axial one.

	jet1	jet2
x_c/D LES	5.0	3.9
x_c/D experiment[15]	7.1	5.5
Ratio	0.70	0.71

Table 2. Comparison between simulated and measured[15] potential core length.

Computed mean axial velocity profiles are compared with experimental data in Figures 2 (a) and (b). Axial distance is normalized by potential core length as $(x - x_c)/x_c$, as proposed by Witze[34]. Velocity decay on the jet axis is well estimated for each case, a slower decrease of jet2 velocity (with respect to normalized distances by the potential core length) being observed numerically and experimentally. Radial profiles of mean axial velocity are plotted in Figure 2 (b), radial distance being classically normalized using half-velocity radius $r_{1/2}$ and momentum thickness δ_θ. Typical similarity properties are pointed out for isothermal and heated jets.

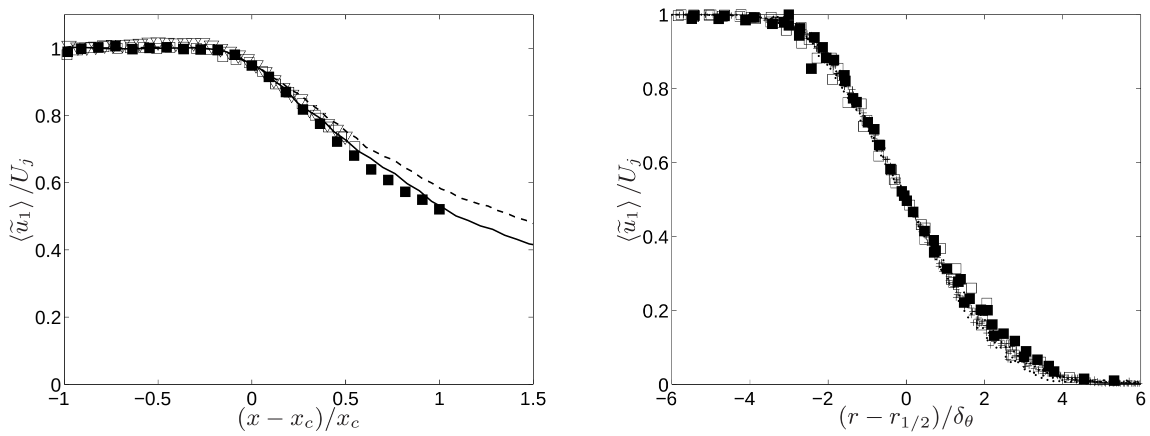

(a) (b)

Figure 2. Mean velocity profiles. (a) **Mean centerline axial velocity. LES: – – – jet1, —— jet2, PIV[11]: ▽ jet1, LDV: □ jet1, ■ jet2.** (b) **Mean velocity radial profiles. Between $x/D = 1$ and 4 for the computation (· jet1, + jet2) and at $x/D = 1$, 2.5 and 5 for LDV measurements[15] (□ jet1, ■ jet2).**

Turbulence intensities $u_{rms} = \sqrt{\widetilde{u}_1''^2}$ and $v_{rms} = \sqrt{\widetilde{u}_2''^2}$ on the jet axis are shown in Figures 3 (a) and (b). Lower levels for simulations in the near-exit region are clearly evidenced, no turbulence being introduced in the exhaust for the computation. Moreover, the evolution of those intensities are consistent with measurements: the levels clearly increase near the end of the potential core to reach a maximum value for $x \approx 1.5\, x_c$. As pointed out experimentally, maximum values of axial intensity are higher for jet2. However, no significant difference for radial intensities is observed numerically, instead of LDV measurements.

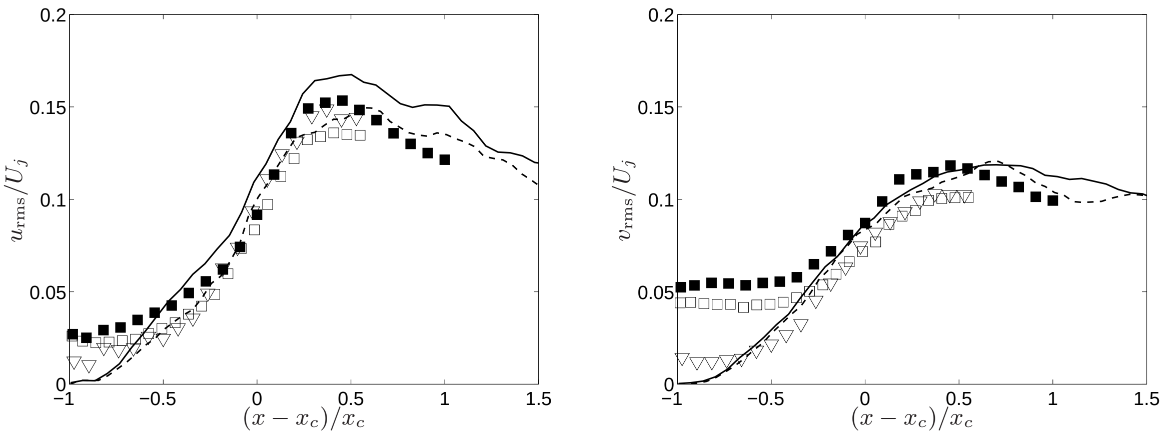

(a) (b)

Figure 3. Mean centerline Reynolds stresses u_{rms} (a) and v_{rms} (b). LES: – – – jet1, —— jet2, PIV:[11] ▽ jet1, LDV:[15] □ jet1, ■ jet2.

IV.B. Velocity spectra

Spectral densities of fluctuating velocity are computed in the mixing layer and on the jet axis from $x/D =$ 0 to 10. To obtain smoother spectra, Welch's method[33] is used, which corresponds to a classical periodogram technique averaged with a 50% overlap. Thus, the temporal signal is windowed with overlapping, and Fourier transforms on each window is computed. Finally, spectral densities are averaged to obtain the PSD. Spectral densities of the fluctuating axial velocity at $x = 10\, D$ in the shear layer (a) and on the jet axis (b) are shown in Figure 4. A quite similary shape is found for spectra, indicating that turbulence is fully developed at $x = 10\, D$ and presents a more universally behaviour in this region. The Kolmogorov law as $f^{-5/3}$ is also observed until a critical Strouhal value St ≈ 0.8. For higher values, numerical dissipation becomes too important and spectra are then affected.

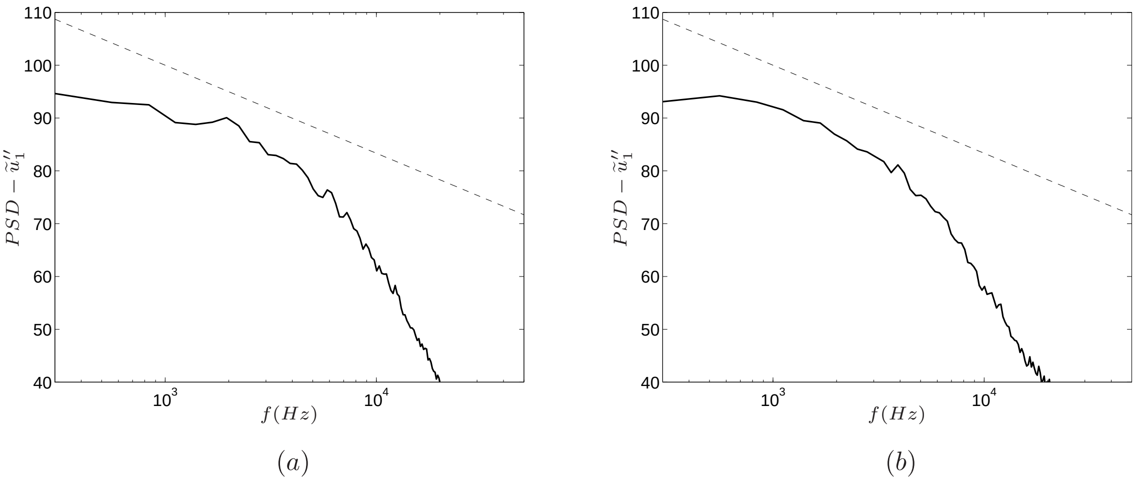

Figure 4. Fluctuating velocity power spectral density on jet axis (a) and in the shear layer (b) at $x = 10\,D$. —— LES, – – – Kolmogorov theoretical decrease as $f^{-5/3}$.

IV.C. Correlations and turbulent scales

To further investigate the instantaneous flow field, second-order space-time correlations R_{ij} are computed for jet1 case. For a displacement $\vec{\xi}$ and a time delay τ, the space-time correlation function between fluctuating velocities u'_i and u'_j is:

$$R_{ij}(\vec{x}, \vec{\xi}, \tau) = \frac{\left\langle \widetilde{u}''_i(\vec{x}, t)\widetilde{u}''_j(\vec{x} + \vec{\xi}, t + \tau) \right\rangle}{\sqrt{\widetilde{u}''^2_i(\vec{x})\widetilde{u}''^2_i(\vec{x} + \vec{\xi})}}$$

Those correlations are evaluated for $|\xi_i| < 2\,D$, and τ in $[-1.4\text{ms}; 1.4\text{ms}]$. To reduce computation time and data storage, time step for correlations is $20\,\Delta t$, as for acoustic data storage. Finally, time averaging is performed on a full time period $T = 60\,\text{ms}$. Convection velocity and integral length scales are then estimated to characterize the simulated flow. The i-component of fluctuating velocity in j-direction, noted $L_i^{(j)}$, is defined as:

$$L_i^{(j)}(\vec{x}) = \frac{1}{2} \int_{\xi_i^-}^{\xi_i^+} R_{ii}(\vec{x}, \xi_j, 0) d\xi_j$$

with ξ_i^- and ξ_i^+ the first negative and positive displacement for which $R_{ii} = 0$.

IV.C.1. Space-time evolution

Second-order space-time correlations R_{11} and R_{22} in the mixing layer at $x/D = 5$ are plotted in Figure 5. Firstly, peaks corresponding to higher correlation level are moving downstream with a convection velocity following $U_c = 0.67\,U_a$, near from classical values for shear layers of axisymmetrical jets. Moreover, the spatial distribution is stretched in the reference direction, so the axial fluctuating velocity is more correlated in the axial direction and conversely for the radial component. Furthermore, a $30°$ angular direction of stronger correlated levels is clearly identified for R_{11}, as pointed out experimentally by Sabot *et al.*[26] and Fleury *et al.*,[11] even if a lower angle of $18°$ was found by these authors.

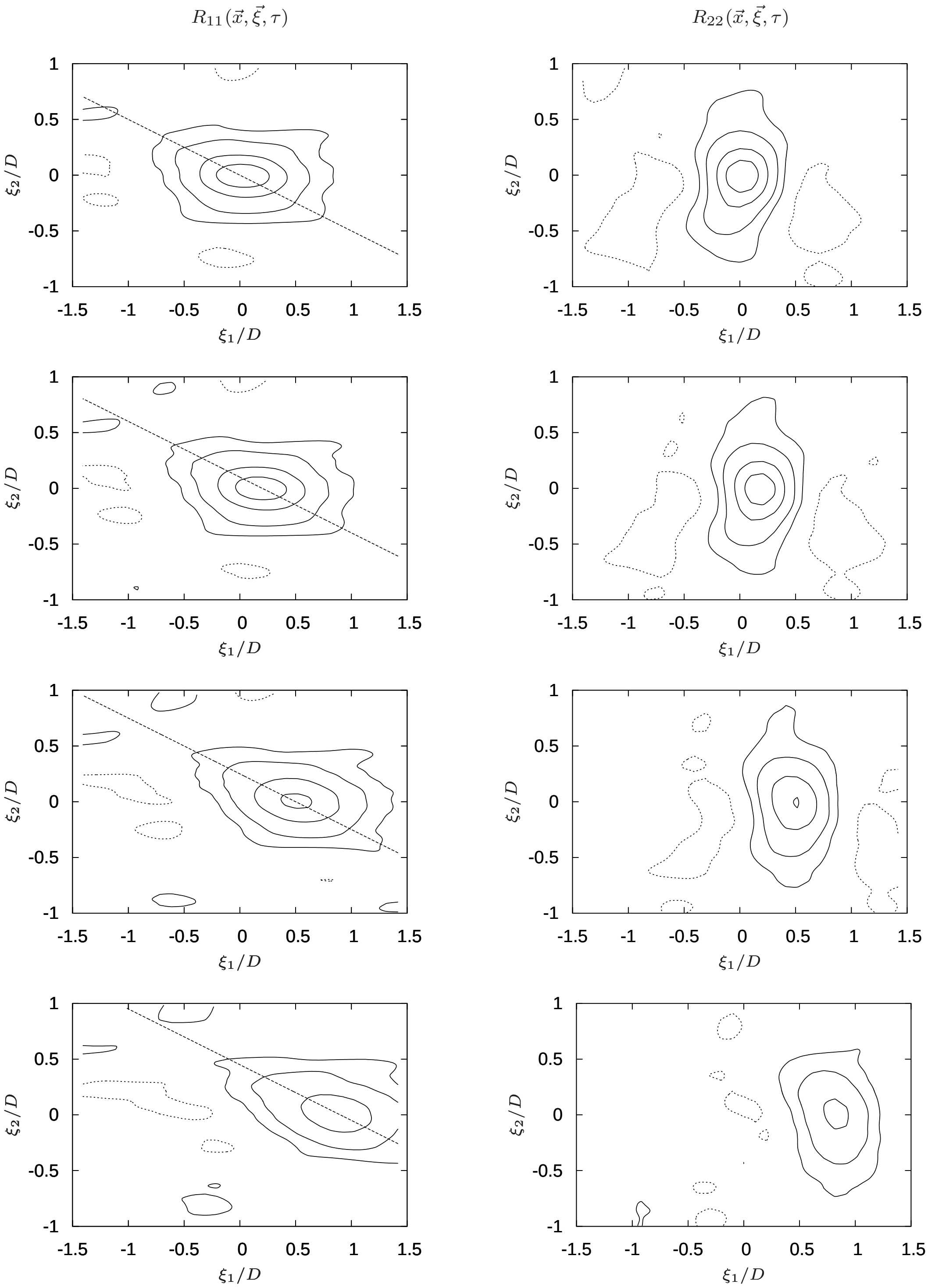

Figure 5. Temporal evolution of R_{11} and R_{22} in the shear layer at $x = 5\,D$. From top to bottom: $\tau = 0, 50, 150$ and $250\,\mu$s. Correlation levels: —— $0.75,\ 0.5,\ 0.25,\ 0.1$; $\cdots\ -0.1$, – – – **Principal direction of correlation.**

IV.C.2. Integral length scales

Axial evolution of integral length scales is represented in Figure 6. With respect to normalized distances by the potential core length, length scales are quite well estimated in comparison to measurements of Fleury *et al.*[11] or Pokora *et al.*[24]. For length scales in radial direction $L_1^{(2)}$, results are also consistent with the empirical law proposed by Liepmann *et al.*[19]. However, for scales in axial direction $L_1^{(1)}$, the relation mentioned by Davies *et al.*[9] is not followed, as for experimental data referenced here. Thus, an update of the source correlation function proposed in Tam & Auriault's fine scale turbulence noise should be performed.

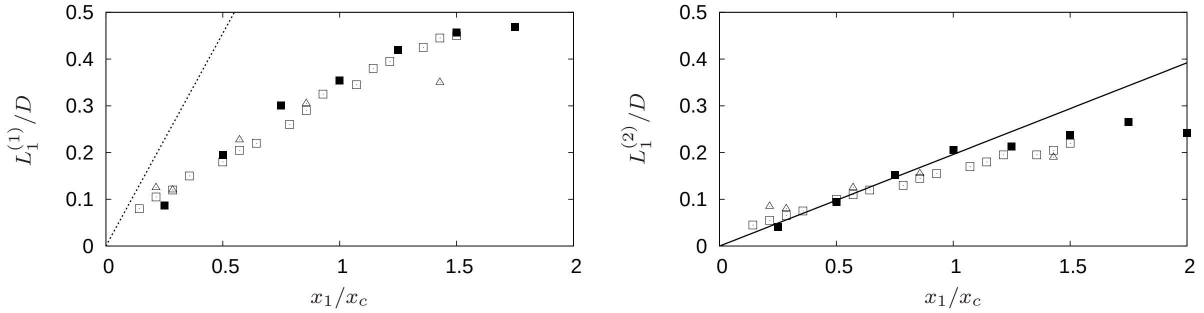

Figure 6. Axial evolution of integral length scales $L_1^{(1)}/D$ and $L_1^{(2)}/D$ in the shear layer ($x_2 = 0.5\,D$) for jet1. ■ LES, □ Fleury[11], △ Pokora[24], ··· Davies *et al.*[9] ($L_1^{(1)} = 0.13\,x_1$), ——— Liepmann *et al.*[19] ($L_1^{(2)} = 0.028\,x_1$).

V. Acoustic results

V.A. Acoustic field

An instantaneous acoustic pressure field and control surface locations are displayed in Figure 7. Acoustic surfaces are located very close to the jet, in order to minimize dissipation effects. However, these surfaces are not too close, to avoid fluctuating aerodynamic structures passing through the surface, as discussed by Rahier *et al.*[25]. Here, turbulent structures are presented with the well-known Q-criterion, defined as $Q = \frac{1}{2}(\widetilde{\omega}_{ij}\widetilde{\omega}_{ij} - \widetilde{s}_{ij}\widetilde{s}_{ij})$ with $\widetilde{s}_{ij}$ and $\widetilde{\omega}_{ij}$ respectively the symmetric and antisymmetric parts of the velocity-gradient tensor.

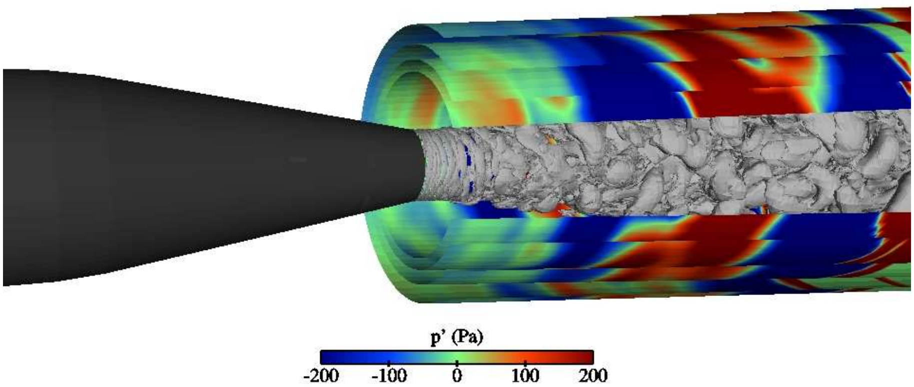

Figure 7. Instantaneous acoustic field on control surfaces and isosurface of Q-criterion ($Q = 10^6\ \mathrm{s}^{-2}$) for jet1 case.

V.B. Influence of the surface location

Four control surfaces are displayed around the jet plume. They all start at the nozzle exit ($x/D = 0$) and end at $x/D = 25$, and differ by their radial position, detailed in Table 3. Note that nearest-furthest surface distance is less than $1\,D$, so that no significant effect of those surface locations is expected.

	S1	S2	S3	S4
r/D at $x/D = 0$	1.95	1.68	1.47	1.31
r/D at $x/D = 25$	3.94	3.66	3.42	3.22

Table 3. Location of acoustic control surfaces.

Typical acoustic pressure field obtained on control surfaces is shown in Figure 7. Isosurface of Q-criterion is also plotted to evaluate vortex location with respect to acoustic surfaces. Qualitatively speaking, control surfaces seem to be far enough to englobe acoustic sources. This conjecture is confirmed by looking at time acoustic pressure signal (a) and power spectral densities (b) obtained in the far field ($r = 30\,D$) for inlet angle $\theta = 120°$ in Figure 8. Time acoustic pressure signals are very similar, small discrepancies for high frequencies are observed on located peaks due to numerical dissipation effect. The effect on power spectral densities is very low, as shown in solid lines in Figure 8(b). Little difference is only visible for frequencies higher than the cut-off one, where numerical dissipation become dominant and so noise levels are stronger for nearest surface and conversely.

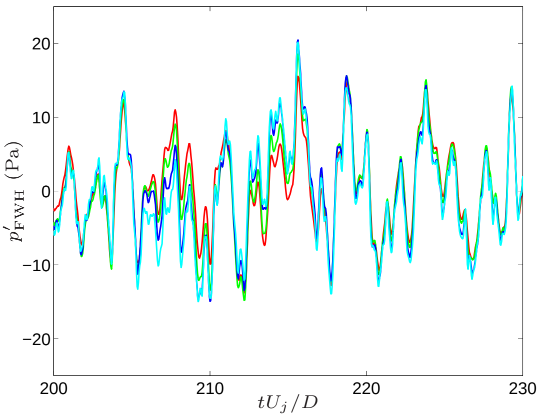

(a)

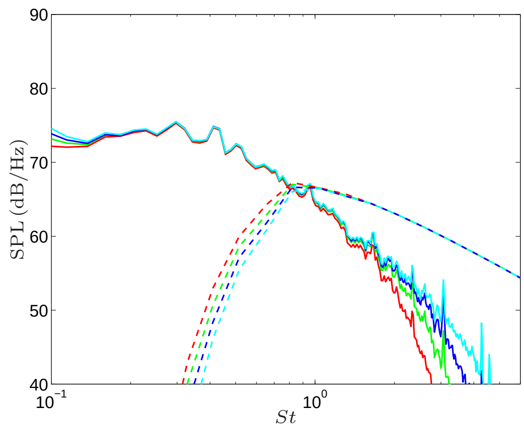

(b)

Figure 8. (a) Time acoustic pressure signals at $\theta = 120°$ and $r/D = 30$ for jet1 case. (b) Surface location influence on power spectral densities at the same observation point. —— $\mathrm{SPL_{LF}}$, – – – $\mathrm{SPL_{HF}}$. Color legend for both figures: —— S1, —— S2, —— S3, —— S4.

Filtered fine-scale noise turbulence is also represented by dashed lines in Figure 8(b). The filtering effectively occurs at the cut-off frequency and same spectra are obtained for higher frequencies. However, the surface influence for lower frequencies is quite consistent with expectations, power spectral densities being higher for the furthest surface, to balance FWH spectra. No significant effect is observed in the present case, but the filtering procedure could be more relevant for more distant surfaces.

V.C. Noise levels

In what follows, only results from surface $S1$ are considered. Sound Pressure Levels obtained in the far field by the coupling methodology are shown in Figure 9 for 4 inlet angles θ, from 60° to 150°. Firstly, low frequency noise levels are overestimated by 3 to 4 dB for every angle. The faster mixing observed in simulations directly contributes to this phenomenon, turbulent levels being stronger and inducing higher pressure fluctuations. As pointed out for the flow field results, this is linked to an unsufficient refined mesh in the mixing layer. However, this overestimation is constant for every angle and low frequency directivity pattern is well evaluated.

For higher frequencies, the filtered fine scale turbulence noise model gives satisfactory results for inlet angles lower than $\theta = 120°$. Higher angles deal with the cone of silence zone, for which the simple directivity factor is not valid any more. Indeed, refraction effects of jet noise sources introduce a strong shape modification of spectra for those angles. As an example, Tam *et al.*[32] recently insisted that the directional dependance of peak Strouhal value is clearly modified when angles become higher than $\theta = 120°$.

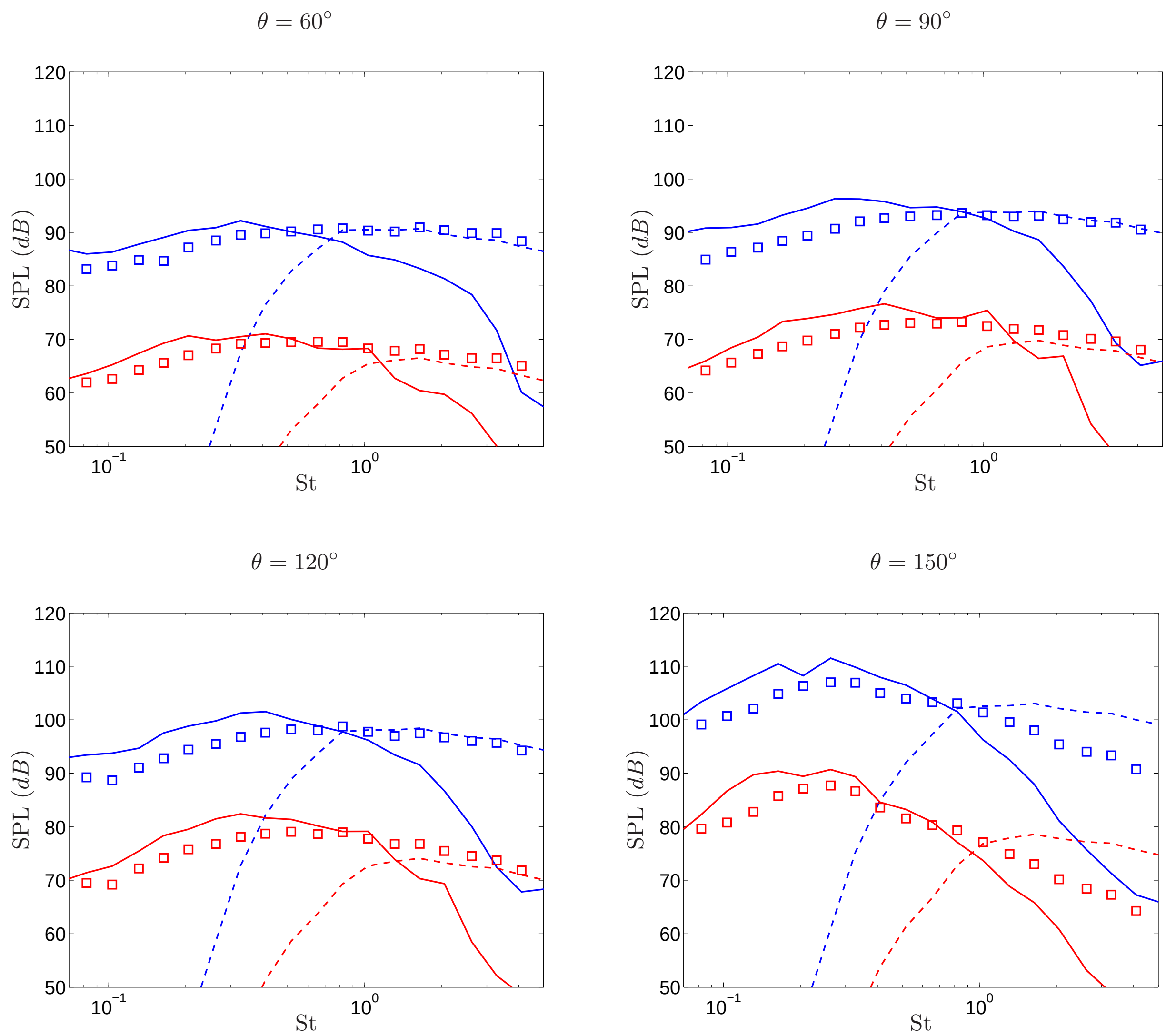

Figure 9. Third-octave Sound Pressure Levels at $r = 30\,D$ for jet1 and jet2 cases with S_1 data. □ measurements, —— $\mathrm{SPL_{LF}}$, – – – $\mathrm{SPL_{HF}}$. Noise levels of jet2 case are shifted by $-20\,$dB.

Predicted and measured noise directivity are presented in Figure 10. The agreement between the simulation and the experiment is satisfactory, even if a 4 dB overestimation is observed. Moreover, sound pressure levels are less overpredicted for forward angles, because of a lack of information near the nozzle exit, acoustic surfaces only starting in the nozzle exit plane. In future simulations, acoustic surfaces will start few diameters upstream to evaluate acoustic radiation for low inlet angles.

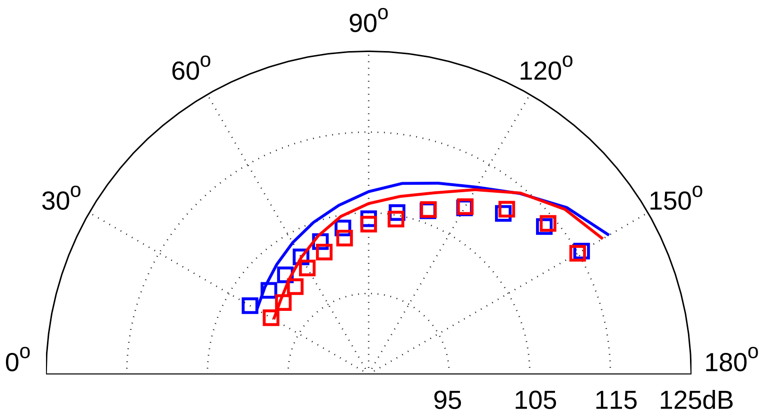

Figure 10. Overall Sound Pressure Levels (OASPL) at $r = 30\,D$ for jet1 and jet2 cases with S_1 data. □ measurements, —— coupling methodology.

VI. Conclusion

A coupling acoustic methodology to evaluate jet noise has been discussed in this paper. Applied to Large Eddy Simulations, this technique provides far field full frequency spectra by merging the Wave Extrapolation Method proposed by Ffowcs-Williams & Hawkings and Tam & Auriault's fine-scale turbulence noise. The turbulent mean field is reconstructed via LES solution. Moreover, a frequency filtering procedure was developped to remove the low frequency part of fine-scale turbulence noise, already computed with the other method.

Two $M = 0.9$ subsonic jets were simulated to evaluate the present model. Even if an overmixing is observed in both simulations, velocity profiles and turbulent length scales are quite satisfactory by using normalized distances by the potential core length. However, turbulent levels are overestimated and leads to higher noise levels than expected. This 4 dB overprediction is observed at low frequencies for all inlet angles, then giving good directivity tendancies. In addition, noise levels for higher frequencies are well evaluated, filtered fine scale turbulence noise providing relevant levels after the cut-off frequency, to complete the power spectral density spectrum.

To improve the coupling methodology presented in this paper, the direct use of computed correlation functions in the fine-scale turbulence model will be investigated, as proposed by Karabasov *et al.*[16] This coupling methodology will also be studied on dual-stream nozzles and chevrons or microjets exhausts. Encouraging results were already obtained on a first application to confluent nozzle.

Acknowledgments

This work has been supported by SNECMA and Ecole Centrale de Lyon. The authors gratefully acknowledge C. Bogey and V. Fleury for providing experimental results.

References

[1] Andersson, N., Eriksson, L. & Davidson, L., Large-eddy simulation of subsonic turbulent jets and their radiated sound, *AIAA Journal*, 2005, Vol. 43, p. 1899-1912.

[2] Bailly, C., Lafon, P. & Candel, S., Subsonic and supersonic jet noise predictions from statistical source models, *AIAA Journal*, 1997, Vol. 35(11), p. 1688-1696.

[3] Bodony, D. J. & Lele, S. K., On using large-eddy simulation for the prediction of noise from cold and heated turbulent jets, *Phys. Fluids*, 2005, Vol. 17(8).

[4]Bogey, C. & Bailly, C., Noise investigation of a high subsonic, moderate Reynolds number jet using a compressible LES, *Theoret. Comput. Fluid Dynamics*, 2003, Vol. 16(4), p. 273-297.

[5]Bogey, C. & Bailly, C., A family of low dispersive and low dissipative explicit schemes forflow and noise computation, *Journal of Computational Physics*, 2004, Vol. 194, p.194-214.

[6]Bogey, C. & Bailly, C., Computation of a high Reynolds number jet and its radiated noise using large-eddy simulation based on explicit filtering, *Computers and Fluids*, 2006, Vol. 35, p. 1344-1358.

[7]Brentner, K. S. & Farassat, F., Modeling aerodynamically generated sound of helicopter rotors, *Progress in Aerospace Science*, 2003, Vol. 39, p. 83-120.

[8]Casalino, D., An advanced time approach for acoustic analogy predictions, *Journal of Sound and Vibration*, 2003, Vol. 261, p. 583-612.

[9]Davies, P. O. A. L., Fisher, M. J. & Barratt, M. J., 1963, The Characteristics of the Turbulence in the Mixing Region of a Round Jet, *Journal of Fluid Mechanics*, **15**, 337-367.

[10]Ffowcs-Williams, J. E. & Hawkings, D. L., Sound generation by turbulence and surfaces in arbitrary motion, *Phil. Trans. Roy. Soc. London*, 1969, Vol. 1151, Ser. A, p. 321-342.

[11]Fleury, V. , Bailly, C., Juvé, D., Michard, M. & Jondeau, E., 2008, Space-time correlations in two subsonic jets using dual-PIV measurements, *AIAA Journal*, **46(10)**, 2498-2509.

[12]Goldstein, M. E., Aeroacoustics, 1976, McGraw-Hill.

[13]Huber, J., 2007, Jet noise assessment and sensitivity at aircraft level, AIAA Paper 2007-3728, 1-11.

[14]Huet, M., Vuillot, F. & Rahier, G., Numerical study of the influence of temperature and micro-jets on subsonic jet noise, *14th AIAA/CEAS Aeroacoustics Conference*, 2008, N° 2008-3029, Vancouver, British Columbia Canada.

[15]Jordan, P. & Gervais, Y., Final Results from single-point measurements, *European project Jet Exhaust Aerodynamics and Noise*, Delivrable 3.4, 2003.

[16]Karabasov, S.A., Afsar, M.Z., Hynes, T.P., Dowling, A.P., McMullan, W.A., Pokora, C.D., Page, G.J. & McGuirk, J.J., Using Large Eddy Simulation within an Acoustic Analogy Approach for Jet Noise Modelling, *14th AIAA/CEAS Aeroacoustics Conference*, 2008, N° 2008-2985, Vancouver, British Columbia Canada.

[17]Khavaran, A. & Bridges, J., 2005, Modelling of fine-scale turbulence mixing noise, *Journal of Sound and Vibration*, Vol. 279(3-5), p. 1131-1154.

[18]Lew, P., Blaisdell, G. A. & Lyrintzis, A. S., Recent progress of hot jet aeroacoustics using 3D Large Eddy Simulation, *11th AIAA/CEAS Aeroacoustics Conference*, 2005, N° 2005-3084, Monterey, California, USA.

[19]Liepmann, H. W. & Laufer, J., 1947, Investigation of free turbulent mixing, *NACA Technical note*, N°1257.

[20]Lighthill, M. J., On sound generated aerodynamically - I General theory, *Proc. Roy. Soc. London*, 1952, Vol. 1107, Ser. A, p. 564-587.

[21]Lupoglazoff, N., Rahier, G. & Vuillot, F., Application of the CEDRE unstructured flow solver to jet noise computations, *European Conference for Aerospace Sciences (EUCASS)*, 2005, Moscou, Russie.

[22]McMullan, W. A., Pokora, C. D., Page, G. J. & McGuirk, J. J., Large Eddy Simulation of a High Reynolds Number Subsonic Turbulent Jet for Acoustic Source Capture, *14th AIAA/CEAS Aeroacoustics Conference*, 2008, N° 2008-2974, Vancouver, British Columbia Canada.

[23]Morris, P. J. & Farassat, F., Acoustic analogy and alternative theories for jet noise prediction, AIAA Journal, 2002, Vol. 40, p. 671-680

[24]Pokora, C. D. & McGuirk, J. J., 2008, Spatio-temporal turbulence correlations using high-speed PIV in an axisymmetric jet, *14th AIAA/CEAS Aeroacoustics Conference*, N°2008-3028.

[25]Rahier, G., Prieur, J., Vuillot, F., Lupoglazoff, N. & Biancherin, A., Investigation of integral surface formulations for acoustic post-processing of unsteady aerodynamic jet simulations, *Aerospace Science and Technology*, 2004, Vol. 8, p. 453-467.

[26]Sabot, J. & Comte-Bellot, G., Courbes d'iso-corrélations spatiales et d'iso-corrélations temporelles relatives aux fluctuations longitudinales de vitesse en conduite lisse circulaire, *Les Comptes Rendus de l'Acadmie des Sciences de Paris*, Oct. 1972, Srie A, Vol. 275(10), p. 667-670.

[27]Smagorinsky, J. S., 1963, General circulation experiments with the primitive equations: I. the basic experiment, *Mon. Weath Rev.*, **91**, 99-163.

[28]Shur, M. L., Spalart, P. R. & Strelets M. K., Noise prediction for increasingly complex jets - Part I: Methods and tests, *International Journal of Aeroacoustics*, 2005, Vol. 4(3), p. 213-246.

[29]Tam, C. K. W. & Auriault, L., Jet mixing noise from fine-scale turbulence, *AIAA Journal*, 1999, Vol. 37(2), p. 145-153.

[30]Tam, C. K. W. & Pastouchenko, N. N., On the two sources of supersonic jet noise, *9th AIAA/CEAS Aeroacoustics Conference*, 2003, N° 2003-3163, Hilton head, South Carolina, USA.

[31]Tam, C. K. W., Dimensional analysis of jet-noise data, *AIAA Journal*, 2006, Vol. 44(3), p. 512-522.

[32]Tam, C. K. W., Viswanathan, K., Ahuja, K. K. & Panda, J., The Sources of Jet Noise: Experimental Evidence, *13th AIAA/CEAS Aeroacoustics Conference*, 2007, N° 2007-3641.

[33]Welch, P. D., The Use of Fast Fourier Transform for the Estimation of Power Spectra: A Method Based on Time Averaging Over Short Modified Periodograms, *IEEE Trans. Audio Electroacoustics*, 1967, Vol. AU-15, p. 70-73.

[34]Witze, P. O., Centerline velocity decay of compressible free jets, *AIAA Journal*, 1974, Vol. 12(4), p. 417-418.

[35]Zhao, W., Frankel, S. & Mongeau, L., Large-eddy simulation of sound radiation from subsonic turbulent jets, *AIAA Journal*, 2001, Vol. 39(8), p. 1469-1477.